

THE AGN POPULATION IN X-RAY SELECTED GALAXY GROUPS AT $0.5 < Z < 1.1$

SEMYEONG OH^{1,8}, JOHN S. MULCHAEY², JONG-HAK WOO^{1,2,9}, ALEXIS FINOGUENOV³, MASAYUKI TANAKA⁴, MICHAEL C. COOPER⁵, FELICIA ZIPARO⁶, FRANZ E. BAUER⁷, KENTA MATSUOKA¹

Draft version June 13, 2014

ABSTRACT

We use Chandra data to study the incidence and properties of Active Galactic Nuclei (AGN) in 16 intermediate redshift ($0.5 < z < 1.1$) X-ray-selected galaxy groups in the Chandra Deep Field-South. We measure an AGN fraction of $f(L_{X,H} > 10^{42}; M_R < -20) = 8.0^{+3.0}_{-2.3}\%$ at $\bar{z} \sim 0.74$, approximately a factor of two higher than the AGN fraction found for rich clusters at comparable redshift. This extends the trend found at low redshift for groups to have higher AGN fractions than clusters. Our estimate of the AGN fraction is also more than a factor of 3 higher than that of low redshift X-ray-selected groups. Using optical spectra from various surveys, we also constrain the properties of emission-line selected AGN in these groups. Contrary to the large population of X-ray AGN ($N(L_{X,H} > 10^{41} \text{ erg s}^{-1}) = 25$), we find only 4 emission-line AGN, 3 of which are also X-ray bright. Furthermore, most of the X-ray AGN in our groups are optically-dull (i.e. lack strong emission-lines) similar to those found in low redshift X-ray groups and clusters of galaxies. This contrasts with the AGN population found in low redshift optically-selected groups which are dominated by emission-line AGN. The differences between the optically and X-ray-selected AGN populations in groups are consistent with a scenario where most AGN in the densest environments are currently in a low accretion state.

Subject headings: galaxies: active — galaxies: groups: general

1. INTRODUCTION

Active Galactic Nuclei (AGN) are now known to play an integral role in galaxy formation and evolution. Although it is established that AGN are powered by the accretion of matter onto supermassive black holes, the trigger mechanism(s) of such nuclear activity is still a matter of debate (e.g., Choi et al. 2009; Lee et al. 2012). The environmental dependence of nuclear activity may provide key clues not only on possible fueling mechanisms but also on the evolution of AGN with changes in environment (e.g., Martini et al. 2007; Shen et al. 2007; Arnold et al. 2009).

One long-standing candidate for triggering of AGN activity is major mergers and interactions between galaxies. Suggested by earlier studies based on the morphologies of quasar host galaxies (Gehren et al. 1984; Heckman et al. 1984; Hutchings & Neff 1992), the merging scenario has also been supported by numerical simulations (e.g., Barnes & Hernquist 1996), and clustering analysis (Henawi et al. 2006; Serber et al. 2006). On the other hand,

various studies of X-ray selected AGN highlight the importance of internal processes, finding no enhancement of AGN activity in interacting galaxies as predicted by merger-driven fueling (cf. Koss et al. 2011). These studies employ various approaches from detailed analysis of host galaxy morphology (e.g., Grogin et al. 2005; Gabor et al. 2009; Cisternas et al. 2011; Böhm et al. 2013; Kocevski et al. 2012) to environmental analysis (e.g., Silverman et al. 2009, 2010). The discrepancies underline the complexity of the matter, including the degeneracies induced by the correlation between galaxy and AGN properties, the need for statistically sound control samples, the likely intrinsic dependence on cosmic epoch, and the different physical scales of environment probed (see Martini 2004, for review).

The incidence of AGN in galaxy groups and clusters provides yet another observational constraint on AGN fueling mechanisms. Naively, there are two main prerequisites to be met for a galaxy with a supermassive black-hole to harbor an AGN: the fuel itself and active feeding mechanisms. Galaxy groups are believed to be particularly conducive to initiate nuclear activity because of the balanced condition between the supply of cold gas and the increased chance of gravitational interaction. Many authors have attempted to study the AGN populations in galaxy groups (Shen et al. 2007; Georgakakis et al. 2008; Arnold et al. 2009; Allevato et al. 2012; Tanaka et al. 2012; Pentericci et al. 2013) and in general these studies are consistent with a higher AGN fraction in groups than in clusters. This would appear to support the idea that galaxies in groups retain larger reservoirs of cold gas to fuel AGN activity than their counterparts in clusters.

Another important question is how AGN activity evolves in time. There has been considerable effort to measure the AGN fraction in groups and clusters at higher redshifts. Eastman et al. (2007) was the first to

¹ Astronomy Program, Department of Physics and Astronomy, Seoul National University, Seoul 151-742, Republic of Korea

² Carnegie Observatories, 813 Santa Barbara Street, Pasadena, CA 91101-1292, USA

³ Department of Physics, University of Helsinki, Gustaf Hallstromin katu 2a, FI-00014 Helsinki, Finland

⁴ National Astronomical Observatory of Japan 2-21-1 Osawa, Mitaka, Tokyo 181-8588, JAPAN

⁵ Center for Galaxy Evolution, Department of Physics and Astronomy, University of California, Irvine, 4129 Frederick Reines Hall Irvine, CA 92697, USA

⁶ School of Physics and Astronomy, University of Birmingham, Edgbaston, Birmingham B15 2TT, UK

⁷ Pontificia Universidad Catolica de Chile, Departamento de Astronomia y Astrofisica, Casilla 306, Santiago 22, Chile

⁸ Current address: Department of Astrophysical Sciences, Princeton University, Princeton, NJ 08544, USA

⁹ Author to whom correspondence should be addressed.

report a significant increase in the cluster AGN population from $z \sim 0.2$ to $z \sim 0.6$. Martini et al. (2009) confirmed this trend up to $z \sim 1$, while Galametz et al. (2009) showed it extends up to at least $z \sim 1.5$. This suggests that the AGN population in rich clusters has experienced substantial evolution due to the cluster environment from $z \sim 1$ to present in a manner similar to star-forming galaxies (Butcher & Oemler 1984). Studies of groups suggest a similar trend with redshift, but with the AGN fraction in groups being higher than clusters at all redshifts studied so far. While the AGN fraction in the field also appears higher than in clusters at low redshift, Martini et al. (2013) find that at $1 < z < 1.5$ the cluster and field AGN fractions are similar. Observations at $z \sim 2 - 3$ suggest the AGN fraction in protoclusters actually exceeds AGN fraction in the field at these redshifts (Lehmer et al. 2009; Digby-North et al. 2010).

Here, we report the incidence and the properties of AGN in 16 X-ray selected groups at $0.5 < z < 1.1$ in the Chandra Deep Field-South (CDFS). Our sample is based on the galaxy group catalog produced by Finoguenov et al. (2014) who searched for extended X-ray emission associated with galaxy groups. An advantage of our study is that the large multi-wavelength datasets in the CDFS provide multiple mass calibrations for these groups which in turn allows us to derive measurements of R_{200} , the radius at which the density becomes 200 times the critical density. This quantity is useful in estimating the virialized part of groups (Connelly et al. 2012) and enables us to explore possible radial trends of AGN properties. Our group sample also benefits from the high spectroscopic completeness in the CDFS. We combine our results with previous studies of the AGN content in groups and clusters to investigate AGN evolution in dense environments. Throughout the paper, we adopt $H_0 = 70 \text{ km s}^{-1} \text{ Mpc}^{-1}$, $\Omega_M = 0.3$, and $\Omega_\Lambda = 0.7$.

2. DATA & SAMPLE

Our groups are taken from the catalog given in Finoguenov et al. (2014). To identify groups, deep images of the CDFS with Chandra (Xue et al. 2011) and XMM-Newton (Comastri et al. 2011) were used to search for extended X-ray emission from the intragroup medium. To detect extended emission, we first remove the flux from point sources following the procedure outlined in Finoguenov et al. (2009, 2010). Point sources are removed separately from the XMM-Newton and Chandra datasets to allow for AGN variability and astrometry differences. The two datasets are combined after the point sources and background has been removed. For the identification of possible galaxy groups, we restrict our analysis to X-ray sources that are extended on a spatial scale of $32''$ or greater.

To verify the emission is associated with a group, we require the system to be detected in optical/near-infrared images. A red sequence finder is used to help identify optical counterparts. We further require that the system be spectroscopically confirmed using the existing redshifts from the CDFS. This analysis results in a sample of 46 X-ray groups spanning a large range of X-ray luminosities ($10^{41} - 10^{43} \text{ ergs s}^{-1}$). A small number of these groups have already been studied by other authors (Tanaka et al. 2013; Ziparo et al. 2013). Here, we focus on 16 groups between $0.5 < z < 1.1$ that are both detected with high

confidence as extended sources in the Chandra images and have good membership data available. We note that three (29, 41, 43) of the groups studied here are in common with the sample of Pentericci et al. (2013) (GS 4, GS 8, GS 5). However, only GS 5 was identified as an X-ray group in their work.

With the location and the approximate redshift of the groups in hand, group members were identified by the method outlined in Mulchaey et al. (2006). For this, we use a compilation of spectroscopic redshifts compiled by the ESO-GOODS team (MASTERCAT_v2.0) with additions from Silverman et al. (2010) and the Arizona CDFS Environment Survey (Cooper et al. 2012). We start by considering all galaxies within $\pm 2000 \text{ km s}^{-1}$ from the approximate redshift of the group, and within a radial distance of R_{200} from the center of the group. From these galaxies, we determine the redshift (\bar{z}) and velocity dispersion (σ_v) of the group. If a galaxy has a radial velocity that is more than $3\sigma_v$ from the new redshift of the group, it is excluded from the group and a new mean redshift and velocity dispersion is calculated. We iterate this process until no further change in group membership is made. In each step, the velocity dispersion (σ_v) of each group is determined using the gapper algorithm (Beers et al. 1990). This process resulted in the elimination of no more than 1 potential group member from any of the groups in our sample. The final group properties are listed in Table 1. The dynamical mass of groups in our sample ranges from $\log M/M_\odot = 12.7$ to $\log M/M_\odot = 14.5$ with the median of $\log M/M_\odot = 13.7$.

We assess the spectroscopic completeness of our group membership using the MUSYC photometric redshift catalog (Cardamone et al. 2010). We apply the same criteria above, and correct the size of each group with the number of additional potential group members found. For each group, we list this corrected size (N), and the size only including galaxies with spectroscopic redshift (N_{spec}) in column 7 and 8 of Table 2. In total, we find 18 additional galaxies that are potential members of these groups, achieving a very high (88%) spectroscopic completeness for galaxies more luminous than $M_R < -20$. Given this high completeness, any missed group members will have a negligible impact on our calculation of the AGN fraction since the Poisson error on the number of AGN dominates the error.

To find X-ray AGN, we match group members with the 4Ms CDFS Source Catalog (Xue et al. 2011). For direct comparison with Eastman et al. (2007), we identify X-ray point sources with rest-frame hard (2-10 keV) X-ray luminosity $L_{X,H} > 10^{42} \text{ erg s}^{-1}$ as AGN. We assume a power-law photon index of 1.8 to convert Chandra absorption-corrected full band luminosity to $L_{X,H}$. Twenty five X-ray point sources are found. All but one of these X-ray sources is associated with a galaxy with a confirmed spectroscopic redshift. The X-ray sources matched with group members and their properties are listed in Table 2.

We also identify emission-line AGN using archival spectra from the literature. Typically, separating AGN from star-forming galaxies requires measurements of the emission line flux ratio $[\text{O III}]/\text{H}\beta$ and $[\text{N II}]/\text{H}\alpha$. In our case, this is not applicable since the wavelength range including $\text{H}\alpha$ - $[\text{N II}]$ is not accessible with the existing

TABLE 1
GROUP PROPERTIES

ID	RA	DEC	Redshift	R ₂₀₀	σ_v	N	N _{spec}	N*	$L_{X,H}^{limit}$
(1)	(deg)	(deg)	(4)	(kpc)	(km s ⁻¹)	(7)	(8)	(9)	($\times 10^{42}$ erg s ⁻¹)
(1)	(2)	(3)	(4)	(5)	(6)	(7)	(8)	(9)	(10)
10	53.00045	-27.90970	0.736498	459	446 ± 38	9	9	7	0.63
20	53.11008	-27.67536	1.040575	500	518 ± 121	8	6	2	1.13
21	53.19170	-27.68820	0.731994	494	362 ± 70	23	20	7	0.52
24	52.98843	-27.70788	0.666333	405	342 ± 189	7	6	3	0.56
25	53.04006	-27.71170	0.733791	453	440 ± 154	8	7	4	0.35
27	53.21977	-27.74213	0.534023	388	258 ± 98	5	5	2	0.14
29	53.07747	-27.79237	0.734147	421	515 ± 148	16	16	7	0.07
30	52.96073	-27.82146	0.679769	559	492 ± 77	19	15	7	0.45
33	53.09682	-27.82853	0.577203	337	259 ± 58	4	4	1	0.03
39	53.27147	-27.86921	0.519614	385	494 ± 223	8	7	3	0.30
41	53.07577	-27.87383	1.096602	349	375 ± 171	7	6	5	0.40
43	53.07750	-27.90421	0.964226	388	277 ± 104	10	8	3	0.51
44	53.02336	-27.91458	0.681612	478	969 ± 276	11	11	4	0.43
63	53.08536	-27.74331	0.523297	378	327 ± 309	3	3	1	0.06
68	53.12672	-27.88589	0.645020	313	157 ± 99	4	4	0	0.12
76	53.21918	-27.70786	1.029214	412	1140 ± 381	8	5	3	1.15

NOTE. — Columns: (1) Identification number; (2, 3) RA, DEC (J2000) of the group position defined as the center of the diffuse X-ray emission; (4) Group redshift; (5) R₂₀₀; (6) Velocity dispersion of the group derived using the gapper algorithm. Errors were estimated using a jackknife method.; (7) The number of group members with $M_R < -20$; (8) The number of spectroscopically confirmed group members with $M_R < -20$; (9) The number of group members with $M_R < M_R^* + 1$; (10) The X-ray point source luminosity detection limit

spectra for our groups. Instead, we use the classification scheme by Yan et al. (2011), which mitigates the problem by using the rest-frame $U - B$ color in place of the $[\text{N II}]/\text{H}\alpha$ ratio. For all group members with a spectroscopic redshift, we look for archival optical spectra from which the redshift was measured. We found spectra for 104 sources (70%), 68 of which cover the $\text{H}\beta$ – $[\text{O III}]$ wavelength range. When both lines are detected, we measure the $[\text{O III}]/\text{H}\beta$ line ratio by fitting a Gaussian to each line after a polynomial continuum level is subtracted. Otherwise, we infer a 3σ limit from the noise level adjacent to the line of interest. The rest-frame $U - B$ colors are measured using EAZY (Brammer et al. 2008) with redshifts fixed to those determined from spectroscopy.

Finally, we use the existing optical spectra to study the emission-line properties of our X-ray selected AGN. Only two out of twelve X-ray AGN with archival spectra covering $\text{H}\beta$ – $[\text{O III}]$ show emission lines. Therefore, we find that most of the X-ray AGN in our group sample are “optically-dull” similar to those found in rich clusters (Eastman et al. 2007).

3. RESULTS

3.1. The Cosmic Evolution of the AGN Fraction in Groups and Clusters

The determination of the AGN fraction critically depends on the AGN classification scheme and the host galaxy luminosity threshold adopted. Here, we make direct comparisons with previous studies by adopting the same AGN and galaxy luminosity thresholds used in the earlier studies. Through out the paper, the errors quoted for the AGN fractions correspond to the 1σ (68%) confidence interval of the Poisson distribution.

First, we compare our result with Eastman et al. (2007), who reported $f(L_{X,H} > 10^{42}; M_R < -20) = 2.8_{-1.0}^{+1.5}\%$ from a sample of four galaxy clusters at $z \sim 0.6$. We find 25 X-ray sources out of 150 group members, 12 of which have $L_{X,H} > 10^{42}$ erg s⁻¹, yielding an AGN fraction $f(L_{X,H} > 10^{42}; M_R < -20) = 8.0_{-2.3}^{+3.0}\%$. Thus,

TABLE 2
X-RAY SOURCES IN GROUPS

XID	RA	DEC	Z	Group	log $L_{X,H}$
(1)	(2)	(3)	(4)	(5)	(6)
355	53.10779	-27.68006	1.045020	20	42.27
367	53.11046	-27.67664	1.043430	20	43.99
601	53.18929	-27.68250	0.734000 ^a	21	42.04
627	53.19967	-27.69675	0.735700	21	43.49
581	53.18300	-27.70061	0.731780	21	41.73
63	52.99063	-27.70242	0.667960	24	42.64
62	52.98987	-27.71442	0.666000	24	42.11
146	53.03825	-27.70722	0.734000	25	42.39
148	53.03929	-27.70994	0.729000	25	41.93
151	53.04054	-27.71347	0.735040	25	41.98
198	53.05775	-27.71369	0.734550	25	43.14
654	53.21687	-27.74014	0.534210	27	41.55
647	53.21379	-27.74158	0.533360	27	41.58
250	53.07517	-27.78856	0.734320	29	41.40
209	53.06183	-27.79408	0.735000	29	41.34
246	53.07346	-27.80336	0.734000	29	41.66
352	53.10729	-27.82686	0.575980	33	41.63
322	53.09863	-27.82736	0.578540	33	40.83
712	53.27346	-27.87056	0.521200	39	42.04
243	53.07163	-27.87250	1.095610	41	44.04
269	53.08029	-27.90189	0.964000	43	42.09
116	53.02492	-27.91397	0.684600	44	41.93
292	53.08871	-27.74336	0.523480	63	41.18
423	53.12567	-27.88500	0.645050	68	41.45
652	53.21608	-27.70825	1.022730	76	42.72

NOTE. — Columns: (1) Chandra 4Ms Source ID; (2, 3) RA, DEC; (4) Redshift; (5) ID of the matched group (see Table 1); (6) Hard band X-ray luminosity;

^a photometric redshift

our estimate for groups at $\bar{z} \sim 0.74$ is larger than that for clusters by more than a factor of 2. This factor is consistent with the one found for groups and clusters at $z \sim 0.043$ (Arnold et al. 2009). If we only consider the 12 groups at $z < 0.8$ ($\bar{z} = 0.65$) in our sample to better match the redshift of the cluster sample, we find the trend is weakened but still present.

We also directly compare our result with low redshift X-ray groups (Arnold et al. 2009). To match the low redshift sample, we limit our sample to groups with $\sigma <$

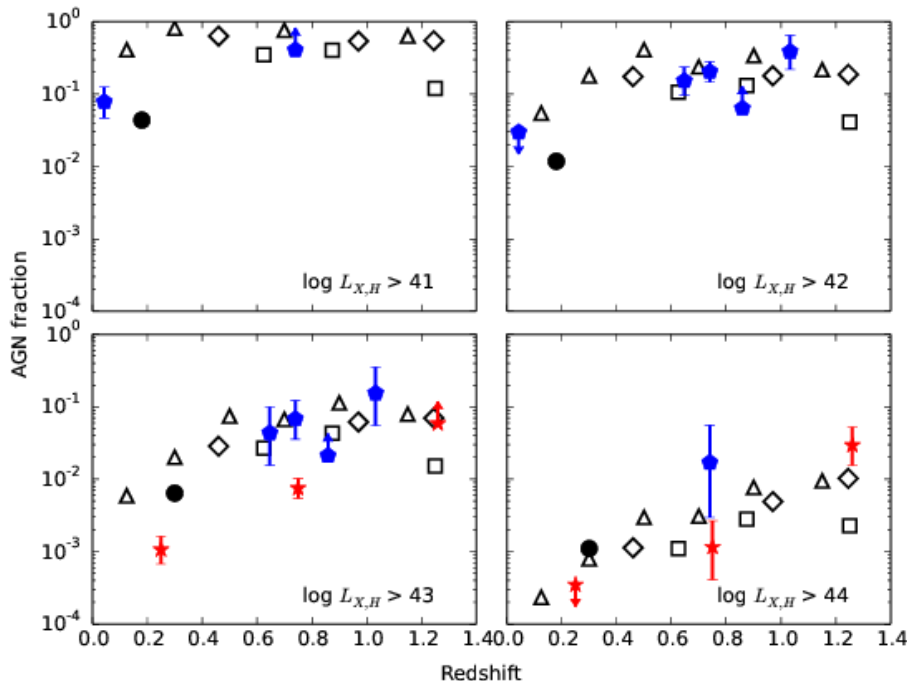


FIG. 1.— Evolution of the AGN fraction in groups (blue pentagon), clusters (red star), and field (black circle). The different panels correspond to different X-ray luminosity thresholds. We divide our sample into low ($\bar{z} = 0.647$) and high ($\bar{z} = 1.033$) redshift bins. AGN fractions for low redshift groups are taken from Arnold et al. (2009), Pentericci et al. (2013) for groups at $z \sim 0.8$, and Martini et al. (2013) for all clusters. We also plot the field AGN fraction from Haggard et al. (2010) at $z \sim 0.2$ (from their Table 4, $f(L_{X,0.5-8 \text{ keV}} > 10^{41}/10^{42}; M_R < -20)$), and at $z \sim 0.3$ as reported by Martini et al. (2013). Field AGN fractions calculated using the field hard X-ray luminosity function (Ueda et al. 2003) and the galaxy luminosity function from Ilbert et al. (2005) (empty circle), Dahlen et al. (2005) (empty triangle), and Chen et al. (2003) (empty square) are also included.

500 km s^{-1} . After converting $L_{X,H}$ to $L_{0.3-8 \text{ keV}}$ using a power-law photon index of 1.8, we find $f(L_{X,0.3-8 \text{ keV}} > 10^{41}; M_R < -20) = 16.8^{+4.9}_{-3.9}\%$ (18/107), a factor of 3 larger than the $5.5^{+2.5}_{-1.8}\%$ (9/164) found for low redshift X-ray groups (Arnold et al. 2009). Note that our estimate is a lower limit to the true value since in many of our groups, we do not reach the depth of $L_{X,H} = 10^{41} \text{ erg s}^{-1}$ used in Arnold et al. (2009) (Table 2). Therefore, like in rich clusters (Martini et al. 2013), the AGN fraction in X-ray groups drops significantly from $z \sim 1$ to the present day.

We also note that our estimate for the AGN fraction in groups is consistent with Pentericci et al. (2013) which recently reported $f(L_{X,H} > 10^{42}; M_R < -20) = 6.3^{+2.1}_{-1.6}\%$ (15/237) using a sample of 11 groups in the GOODS fields at $\bar{z} = 0.859$. Five of the groups in the Pentericci et al. (2013) sample are selected from the CDFS. As noted earlier, three of these groups are in fact X-ray detected and in our sample. Although the Pentericci et al. (2013) sample was not X-ray selected, the high fraction of overlap between our samples in the CDFS field suggests that their detection method is also largely identifying more massive and evolved groups.

In Figure 1, we show the evolution of the AGN fraction in groups and clusters. To properly compare the AGN fraction across redshifts, we need to account for the evolution of the galaxy population. Following Martini et al. (2009), we adopt an evolving galaxy luminosity threshold $M_R < M_R^*(z) + 1$ where $M_R^*(z) = -21.92 - z$. For clusters, we use values from Martini et al. (2013) binned

at $z = 0.25, 0.75$, and 1.26 which includes data from Eastman et al. (2007). As can be seen from Figure 1, the frequency of AGN activity is enhanced in groups over clusters by approximately an order of magnitude for $L_{X,H} > 10^{43} \text{ erg s}^{-1}$. In addition, we find that the AGN fraction in groups increases with redshift. This result is consistent with the trend found for clusters and verifies the result reported by Pentericci et al. (2013) for groups.

Haggard et al. (2010) investigated the AGN fraction in the field to $z = 0.7$ using the *Chandra* Multiwavelength Project and the Sloan Digital Sky Survey. By matching AGN X-ray luminosity and host galaxy R-band magnitude threshold with those of Martini et al. (2007), they find an excellent agreement between the field and cluster AGN fraction at low redshift ($0.05 < z < 0.31$) for relatively low luminosity AGNs ($L_{X,H} \sim 10^{41-42} \text{ erg s}^{-1}$). A somewhat different picture emerges for higher luminosity AGNs ($L_{X,H} \sim 10^{43-44} \text{ erg s}^{-1}$). For these objects, Martini et al. (2013) found that the field AGN fraction is about six times higher than in clusters at low redshift. However, the fractions are comparable in these environment even for luminous AGN by $z \sim 1.25$ (Martini et al. 2013). Here, we find that at $z \sim 0.7$ the AGN fraction for higher luminosity AGNs in groups is significantly higher than that in clusters. Currently, the field AGN fraction based on the selection criteria adopted in this paper at this redshift is not well-constrained and it is unclear whether the AGN fraction in groups is higher than that of field. As a first attempt, we follow Martini

et al. (2009), and calculate the “field” AGN fraction using the field hard X-ray luminosity function of Ueda et al. (2003) and the galaxy luminosity functions from the VIMOS-VLT Deep Survey (Ilbert et al. 2005), the Las Campanas Infrared Survey (Chen et al. 2003), and the Great Observatories Origins Deep Survey (Dahlen et al. 2005). We normalize the number density of hard X-ray sources given from the luminosity-dependent density evolution model by the number density of galaxies brighter than $M_R^*(z) + 1$ where $M_R^*(z)$ is given by each luminosity function. We find that the AGN fraction of our group sample is in general consistent with the field AGN fractions from luminosity functions at all redshifts and luminosity thresholds. However, we caution that these field estimates may be contaminated by galaxies in groups. Nonetheless, the general picture emerges that high luminosity AGNs ($L_{X,H} \sim 10^{43-44} \text{ erg s}^{-1}$) are sensitive to the environment and that the group environment is more favorable for galaxies to host high luminosity AGNs than richer environments like clusters.

3.2. AGN Properties

In this section, we investigate various properties of AGN in our sample, and compare them with previous studies. First, we compare the X-ray and emission-line AGN content of groups and clusters. In contrast to the $> 60\%$ of galaxies in low redshift poor groups showing strong emission lines (Shen et al. 2007), only 8 of 68 galaxies (18%) in our groups with optical spectra covering $H\beta$ -[O III] show measurable emission lines. Of these 8 galaxies, only one galaxy has line ratios consistent with hosting a narrow-line AGN according to the Yan et al. (2011) diagnostics, and this object also has a high X-ray luminosity ($L_{X,H} = 1.4 \times 10^{43} \text{ erg s}^{-1}$). In addition, there are three more AGN candidates detected by their broad Mg II emission in the near-UV or their broad band SEDs. In total, four strong emission-line AGN are found in our group sample, three of which are also X-ray bright. As noted earlier, most of the X-ray AGN in our sample are optically dull similar to the nearly disjoint population of optical and X-ray AGN in X-ray groups at low redshift (Arnold et al. 2009) or X-ray AGN in clusters at similar redshift (Eastman et al. 2007). On the other hand, emission-line AGN appear to be more common than X-ray bright, optically-dull AGN in groups that do not contain a significant intragroup medium component (Shen et al. 2007). These results are consistent with the idea that X-ray bright, optically-dull AGN are more common in more virialized systems, as suggested by some accretion evolution scenarios (Shen et al. 2007).

We are also interested in determining if X-ray AGN have a different spatial distribution in groups than non-AGN hosting galaxies. To determine this, in Figure 2 we show the distribution of non-AGN galaxies and galaxies hosting an X-ray source in a groupcentric distance (r/R_{200})-velocity (v/σ_v) diagram. The velocities are normalized by the rest-frame velocity dispersion of each group. The marginalized distribution of each parameter is also presented in a separate panel respectively for X-ray AGN and non-AGN galaxies. As can be seen from Figure 2, X-ray sources are more centrally concentrated than non-AGN galaxies: 75% of all X-ray sources, and 80% of all X-ray AGN ($L_{X,H} > 10^{42} \text{ erg s}^{-1}$) reside within a half of the R_{200} . Our result is consistent with the

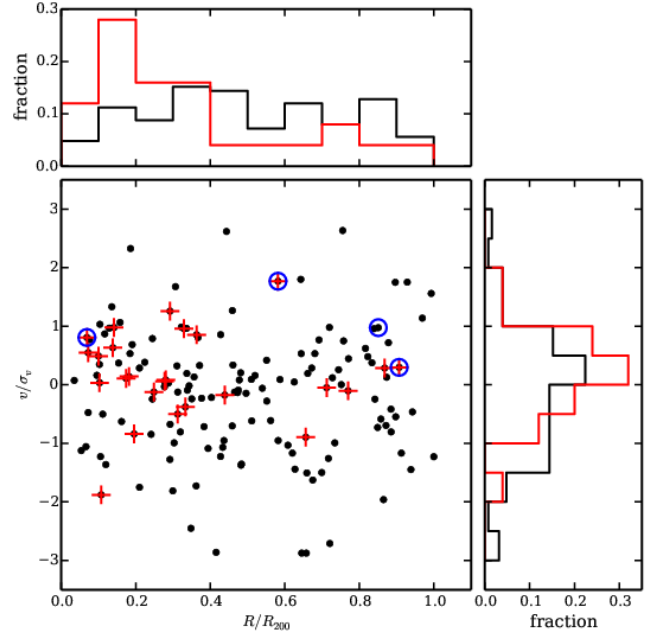


FIG. 2.— Distribution of X-ray AGN (red crosses) and non-AGN galaxies (black points) in the $r/R_{200} - v/\sigma_v$ plane (lower left). Shared axis plots show the marginalized distribution of each parameter for X-ray AGN (red) and non-AGN galaxies (black). Optical AGN are enclosed in blue circles.

central concentration of X-ray sources in clusters (Ruderman & Ebeling 2005; Martini et al. 2007; Galametz et al. 2009; Bignamini et al. 2008). However, our result appears inconsistent with the result of Pentericci et al. (2013) who found that X-ray AGN are preferentially located at the edge of groups and small clusters at similar redshifts. The difference may be due to the different methods used to define the center and extent of each group. In the three groups in common with their sample, we find that the center determined as the peak position of the density distribution of each structure by their algorithm can be offset by as much as $\sim 23''$ from our estimate determined from the X-ray emission. Such a difference may have washed out the trend we see in Figure 2 in the Pentericci et al. (2013) study. We find no difference in the velocity structure of AGN and non-AGN hosting galaxies in groups, consistent with Pentericci et al. (2013). We also find no correlation between X-ray luminosity and groupcentric radial distance or velocity.

3.3. Host Galaxy Properties

The morphologies of AGN host galaxies can provide valuable information on possible fueling mechanisms of nuclear activity. While such studies are often prohibited or biased by the presence of a bright nucleus in QSO host galaxies, most of the X-ray AGN in our sample are optically dull, making it easier to study the morphology of the underlying stellar population. In Figure 3 we present the HST z-band images of all 25 X-ray sources in our group sample using the Galaxy Evolution from Morphologies and SEDs survey (GEMS; Rix et al. 2004). Visual inspection of the X-ray detected galaxies reveal a variety of morphologies. While several galaxies show evidence of nearby companions or merging signatures, the majority shows no clear sign of major merger. Thus,

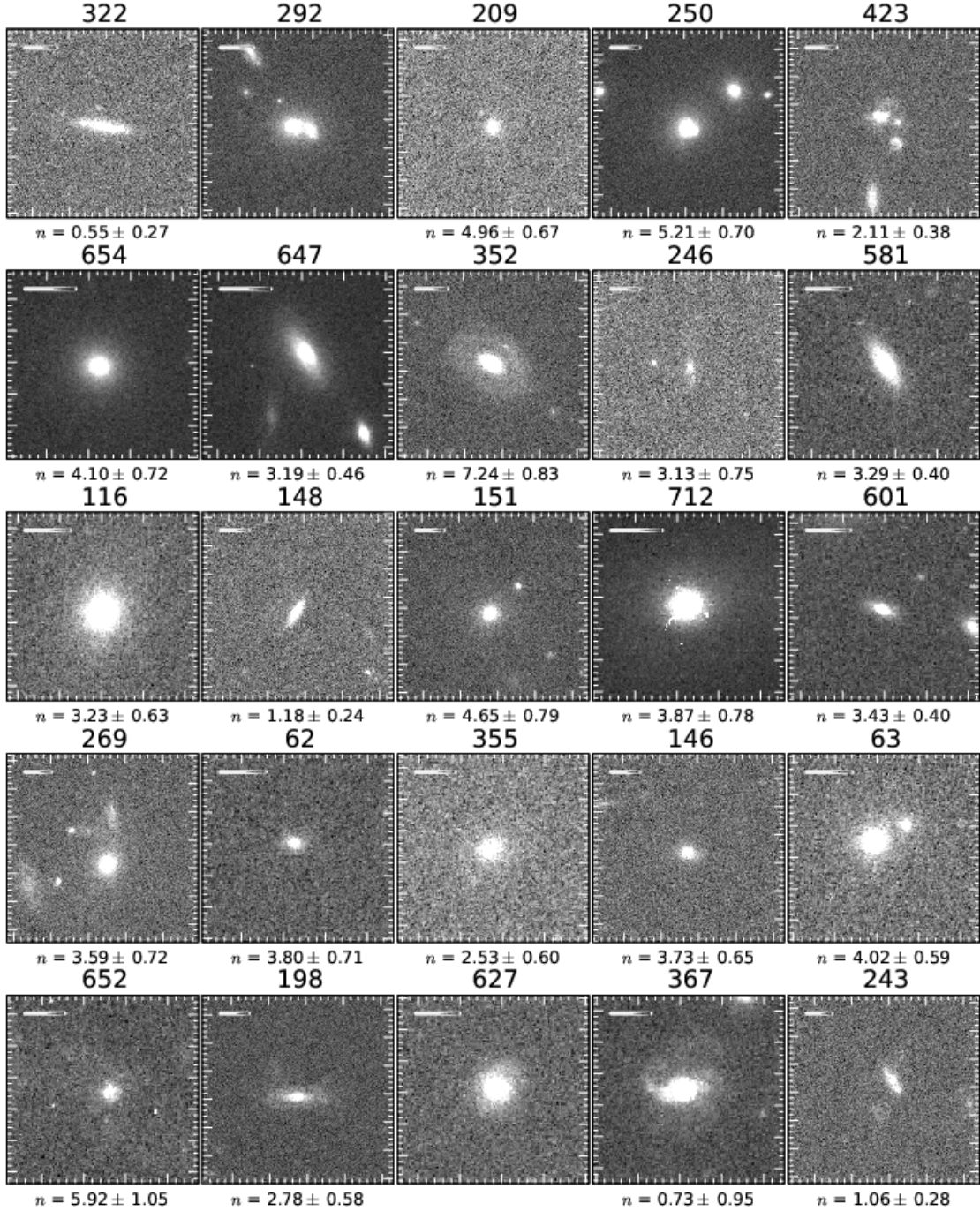


FIG. 3.— GEMS HST z-band images of 25 X-ray AGN ($L_{X,H} > 10^{42}$ erg s $^{-1}$) from our group sample. Each image covers 6×6 arcsec 2 . Scale bars correspond to a physical scale of 10 kpc in each image. The Sersic index from Häussler et al. (2007) is presented at the bottom of each panel.

it seems unlikely that the current AGN activity in these galaxies has been triggered by an on-going major merger. This is consistent with the recent findings that most of moderate-luminosity AGN are not hosted by starbursting major mergers (e.g., Xue et al. 2010; Mullaney et al. 2012).

In Figure 3 we also list the Sersic index on the bottom of each panel if available. These indices are derived from fitting a single Sersic profile component to the HST z-band images (see Häussler et al. 2007). Most of the host galaxies have high Sersic indices with mean

$n = 3.40 \pm 1.59$. Although a single Sersic fit is a somewhat limited way to characterize the complex nature of host galaxies, it does suggest that these galaxies are mostly bulge-dominated. While only one (XID 292) out of 25 X-ray AGN host galaxies is clearly a major merger, this together with the high Sersic indices may indicate that minor mergers or internal processes may have triggered the nuclear activity in these galaxies as minor mergers can also make a significant contribution to the formation of bulges (Hopkins et al. 2010).

To investigate whether the AGN activity in groups is

correlated with star formation, we use 100 and 160 μm flux measurements from the GOODS-Herschel Survey (Elbaz et al. 2011) and PACS Evolutionary Programme (Lutz et al. 2011). We find nine and seven detections, respectively at 100 and 160 μm among our 25 X-ray AGN, and compare them with the X-ray luminosities in Figure 4. We find that compared to low-redshift optical or X-ray selected AGN (e.g., Netzer et al. 2007), the far-infrared (FIR) luminosity is higher at a given AGN luminosity, indicating that AGN in galaxy groups at $z \sim 0.7$ are hosted by galaxies with higher star formation rates than local galaxies. On the other hand, we find no strong correlation between X-ray and FIR luminosity although the FIR-detected sample is small. These results are consistent with the findings of other studies of X-ray detected galaxies. For example, Mullaney et al. (2012) report that moderate-luminosity X-ray AGN ($\log L_X = 42\text{--}44 \text{ erg s}^{-1}$) at similar redshifts show no correlation between star formation and AGN luminosity and that the star formation rate of X-ray AGN host galaxies increases strongly from $z \sim 0$ to 3 (see their Figure 5). This may indicate that X-ray AGN host galaxies in the group environment follow a similar trend of a relative growth of stars and supermassive black holes to the general galaxy population in other environments at the same redshift while the higher X-ray AGN fraction in group galaxies implies that the triggering of AGN and star formation is more frequent in the group environment than in the cluster environment. The higher AGN fraction is presumably due to the larger gas content and favorable conditions for dynamical interaction among member galaxies.

4. SUMMARY

We have studied the X-ray and optical AGN population in 16 X-ray-selected groups at $0.5 < z < 1.1$ in the Chandra Deep Field South. Our sample benefits from the extensive analysis of deep X-ray images of CDFS, and also from the rich archival data available from various sources. Specifically, we achieve high spectroscopic completeness which rules out false positive assignments of AGN to groups. We summarize our results as follows:

- We measure an X-ray AGN fraction of $f(L_{X,H} > 10^{42}; M_R < -20) = 8.0^{+3.0}_{-2.3}\%$ at $z \sim 0.74$. This AGN fraction is higher than that found for similar groups at low redshift.
- Similar to the results found at low redshift, the AGN fraction is higher in groups than in clusters at intermediate redshifts. This result is consistent with the expectation that galaxies in groups contain more cold gas and are more likely to experience an interaction than galaxies in rich clusters.
- Most of the X-ray detected AGN in these groups are optically dull (i.e. do not contain strong emission lines) similar to those found in rich clusters.
- We find that X-ray AGN are more centrally concentrated in groups than non-AGN hosting galaxies. However, we find no apparent trend between the X-ray luminosity of the AGN and the group-centric radial distance or velocity.

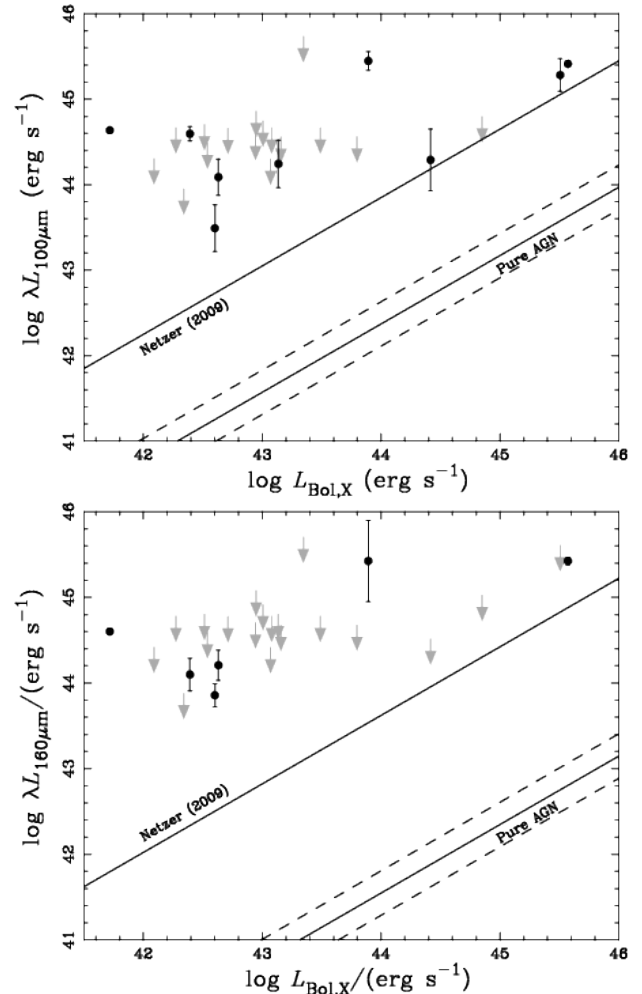


FIG. 4.— Comparison of X-ray based AGN luminosity with 100 μm (top) and 160 μm luminosities (bottom). Although the far-IR detections are limited to a small fraction of the sample (filled circles), no strong correlation is present between X-ray and FIR luminosity. The local relation (solid line) is taken from Netzer et al. (2009) after converting the star formation rate into far-IR luminosity. Note that AGN luminosity has been derived from X-ray luminosity using the bolometric correction method (Rigby et al. 2009). The locus of AGN host galaxies without star formation (pure AGN) is also indicated by a solid line with $1\text{-}\sigma$ dispersion (Mullaney et al. 2011; Rosario et al. 2012).

- The majority of the X-ray AGN host galaxies are bulge-dominated systems. Only one of the 25 galaxies shows clear evidence of an on-going major merger.
- By comparing the far-infrared and X-ray luminosities of X-ray detected galaxies, we find that star formation rate for given AGN luminosity is higher than in local AGN host galaxies. This trend is similar to that of X-ray AGN host galaxies in general (Mullaney et al. 2012), suggesting that the relative growth of stars and supermassive black holes in the group environment is similar to that in other environments.

We thank the anonymous referee for a very helpful report that helped improve this paper. This research has been supported by TJ Park Science Fellow-

ship of POSCO TJ Park Foundation. J.S.M acknowledges partial support for this work from SAO grant SP1-12006A and HST grant AR-12831 J.H.W acknowledges the support by the National Research Foundation of Korea (NRF) grant funded by the Korea gov-

ernment (No. 2012-006087). AF acknowledges support from SAO grant SP1-12006B. M.T acknowledges support by KAKENHI No. 23740144. This research made use of Astropy (<http://www.astropy.org>), a community-developed core Python package for Astronomy and TOP-CAT (<http://www.starlink.ac.uk/topcat/>).

REFERENCES

- Allevato, V., Finoguenov, A., Hasinger, G., et al. 2012, *ApJ*, 758, 47
- Arnold, T. J., Martini, P., Mulchaey, J. S., Berti, A., & Jeltema, T. E. 2009, *ApJ*, 707, 1691
- Barnes, J. E., & Hernquist, L. 1996, *ApJ*, 471, 115
- Beers, T. C., Flynn, K., & Gebhardt, K. 1990, *AJ*, 100, 32
- Bignamini, A., Tozzi, P., Borgani, S., Ettori, S., & Rosati, P. 2008, *A&A*, 489, 967
- Böhm, A., Wisotzki, L., Bell, E. F., et al. 2013, *A&A*, 549, A46
- Brammer, G. B., van Dokkum, P. G., & Coppi, P. 2008, *ApJ*, 686, 1503
- Butcher, H., & Oemler, Jr., A. 1984, *ApJ*, 285, 426
- Cardamone, C. N., van Dokkum, P. G., Urry, C. M., et al. 2010, *ApJS*, 189, 270
- Chen, H.-W., Marzke, R. O., McCarthy, P. J., et al. 2003, *ApJ*, 586, 745
- Choi, Y.-Y., Woo, J.-H., & Park, C. 2009, *ApJ*, 699, 1679
- Cisternas, M., Jahnke, K., Inskip, K. J., et al. 2011, *ApJ*, 726, 57
- Comastri, A., Ranalli, P., Iwasawa, K., et al. 2011, *A&A*, 526, L9
- Connolly, J. L., Wilman, D. J., Finoguenov, A., et al. 2012, *ApJ*, 756, 139
- Cooper, M. C., Yan, R., Dickinson, M., et al. 2012, *MNRAS*, 425, 2116
- Dahlen, T., Mobasher, B., Somerville, R. S., et al. 2005, *ApJ*, 631, 126
- Digby-North, J. A., Nandra, K., Laird, E. S., et al. 2010, *MNRAS*, 407, 846
- Eastman, J., Martini, P., Sivakoff, G., et al. 2007, *ApJ*, 664, L9
- Elbaz, D., Dickinson, M., Hwang, H. S., et al. 2011, *A&A*, 533, A119
- Finoguenov, A., Connolly, J. L., Parker, L. C., et al. 2009, *ApJ*, 704, 564
- Finoguenov, A., Watson, M. G., Tanaka, M., et al. 2010, *MNRAS*, 403, 2063
- Finoguenov, A., Tanaka, M., Cooper, M., Allevato, V., Cappelluti, N., Choi, A., Heymans, C., Bauer, F.E., et al. 2014, *A&A*, submitted
- Galametz, A., Stern, D., Eisenhardt, P. R. M., et al. 2009, *ApJ*, 694, 1309
- Gabor, J. M., Impey, C. D., Jahnke, K., et al. 2009, *ApJ*, 691, 705
- Georgakakis, A., Gerke, B. F., Nandra, K., et al. 2008, *MNRAS*, 391, 183
- Gehren, T., Fried, J., Wehinger, P. A., & Wyckoff, S. 1984, *ApJ*, 278, 11
- Grogin, N. A., Conselice, C. J., Chatzichristou, E., et al. 2005, *ApJ*, 627, L97
- Haggard, D., Green, P. J., Anderson, S. F., et al. 2010, *ApJ*, 723, 1447
- Häussler, B., McIntosh, D. H., Barden, M., et al. 2007, *ApJS*, 172, 615
- Heckman, T. M., Bothun, G. D., Balick, B., & Smith, E. P. 1984, *AJ*, 89, 958
- Hennawi, J. F., Strauss, M. A., Oguri, M., et al. 2006, *AJ*, 131, 1
- Hopkins, P. F., Bundy, K., Croton, D., et al. 2010, *ApJ*, 715, 202
- Hutchings, J. B., & Neff, S. G. 1992, *AJ*, 104, 1
- Ilbert, O., Tresse, L., Zucca, E., et al. 2005, *A&A*, 439, 863
- Kocevski, D. D., Faber, S. M., Mozena, M., et al. 2012, *ApJ*, 744, 148
- Koss, M., Mushotzky, R., Veilleux, S., et al. 2011, *ApJ*, 739, 57
- Lee, G.-H., Woo, J.-H., Lee, M. G., et al. 2012, *ApJ*, 750, 141
- Lehmer, B. D., Alexander, D. M., Geach, J. E., et al. 2009, *ApJ*, 691, 687
- Lutz, D., Poglitsch, A., Altieri, B., et al. 2011, *A&A*, 532, A90
- Martini, P. 2004, in *IAU Symposium*, Vol. 222, *The Interplay Among Black Holes, Stars and ISM in Galactic Nuclei*, ed. T. Storchi-Bergmann, L. C. Ho, & H. R. Schmitt, 235–241
- Martini, P., Mulchaey, J. S., & Kelson, D. D. 2007, *ApJ*, 664, 761
- Martini, P., Sivakoff, G. R., & Mulchaey, J. S. 2009, *ApJ*, 701, 66
- Martini, P., Miller, E. D., Brodwin, M., et al. 2013, *ApJ*, 768, 1
- Mulchaey, J. S., Lubin, L. M., Fassnacht, C., Rosati, P., & Jeltema, T. E. 2006, *ApJ*, 646, 133
- Mullaney, J. R., Alexander, D. M., Goulding, A. D., & Hickox, R. C. 2011, *MNRAS*, 414, 1082
- Mullaney, J. R., Pannella, M., Daddi, E., et al. 2012, *MNRAS*, 419, 95
- Pentericci, L., Castellano, M., Menci, N., et al. 2013, *A&A*, 552, A111
- Rigby, J. R., Diamond-Stanic, A. M., & Aniano, G. 2009, *ApJ*, 700, 1878
- Rix, H.-W., Barden, M., Beckwith, S. V. W., et al. 2004, *ApJS*, 152, 163
- Rosario, D. J., Santini, P., Lutz, D., et al. 2012, *A&A*, 545, A45
- Ruderman, J. T., & Ebeling, H. 2005, *ApJ*, 623, L81
- Serber, W., Bahcall, N., Ménard, B., & Richards, G. 2006, *ApJ*, 643, 68
- Shen, Y., Mulchaey, J. S., Raychaudhury, S., Rasmussen, J., & Ponman, T. J. 2007, *ApJ*, 654, L115
- Silverman, J. D., Kovač, K., Knobel, C., et al. 2009, *ApJ*, 695, 171
- Silverman, J. D., Mainieri, V., Salvato, M., et al. 2010, *ApJS*, 191, 124
- Silverman, J. D., Kampeczyk, P., Jahnke, K., et al. 2011, *ApJ*, 743, 2
- Tanaka, M., Finoguenov, A., Lilly, S. J., et al. 2012, *PASJ*, 64, 22
- Tanaka, M., Finoguenov, A., Mirkazemi, M., et al. 2013, *PASJ*, 65, 17
- Ueda, Y., Akiyama, M., Ohta, K., & Miyaji, T. 2003, *ApJ*, 598, 886
- Xue, Y. Q., Luo, B., Brandt, W. N., et al. 2011, *ApJS*, 195, 10
- Yan, R., Ho, L. C., Newman, J. A., et al. 2011, *ApJ*, 728, 38
- Ziparo, F., Popesso, P., Biviano, A., et al. 2013, *MNRAS*, 1855